

**Analysis of the Large
Gamma Ray Flares
of
Mkn 421
as Observed with HEGRA CT1
on the Island La Palma
in 2001**

Ph.D. Thesis

by

Thomas Schweizer

supervised by

Manel Martinez
IFAE
Edifici Cn., UAB
08193 Bellaterra/Spain

and

Eckart Lorenz
Max Planck Institut für Physik
80805 München/Germany

Acknowledgements

First, I wish to sincerely thank my supervisors Dr. Manel Martinez from the Institut de Fisica d'Altes Energies/Spain and Dr. Eckart Lorenz from the Max Planck Institut für Physik in Munich for supervising and providing me with this interesting Ph.D. subject and for giving me a chance to do real physics for my doctoral work. Both helped me immensely by providing me with the necessary work environment and giving me the possibility to participate in several conferences and schools. In addition, they always helped me with questions and problems related to physics and last but not least for cross-reading this thesis. Dr. Eckart Lorenz provided me with an abundance of long distance support via many fruitful discussions and invitations to Munich. Without his help it would have been much more difficult to accomplish good results. Many of the ideas in this work, like weights in the calculation of Hillas parameters, and several more came from him.

I also wish to thank Enrique Fernandez very much for providing me with the opportunity to do a doctoral thesis at IFAE, to live in Spain and to learn about and experience two fascinating cultures, the Catalan one and the Spanish one.

In addition I would like to thank all the members of the HEGRA collaboration for supplying me with the astronomical data. I am grateful to all the HEGRA members of the Max Planck Institut für Physik in München that I have known personally, for very good cooperation and for teaching me an abundance of valuable information about Cherenkov Telescopes, especially the CT1. These people include Razmik Mirzoyan, Martin Kestel, Daniel Kranich and Juan Cortina. I owe special thanks to Wolfgang Wittek for some very helpful discussions and for cross-reading my thesis.

At this point I wish to sincerely thank Kristo Karr for the painful English correction of my thesis. Without him the thesis would not be what it is now! The other cross readers must also to be mentioned here. These people are Markus Gaug and Martin Kestel.

At IFAE I wish to thank Markus Gaug, David Paneque, Josep Flix, Javier Lopez, Eva Domingo and Oscar Blanch for their good team work and for providing a very nice working environment at the institute. In this context I owe special thanks to Sacha Ostankov with whom I had a very pleasant and productive working collaboration.

Finally, I wish to extend my most heartfelt thanks to my wife Miha who supported me with her love, which provided me with the energy needed to accomplish this work. Another heartfelt thanks to my parents for supporting my studies in physics, helping me during difficult times and for providing steadfast moral support.

Contents

| | | |
|----------|--|-----------|
| 1 | Introduction to the theory and detectors | 11 |
| 1.1 | Cosmic rays | 11 |
| 1.1.1 | The spectrum of cosmic rays | 12 |
| 1.1.2 | Sources of cosmic rays | 12 |
| 1.1.3 | γ -rays and γ -ray production processes | 13 |
| 1.2 | Active galactic nuclei and the class of BL LACs | 14 |
| 1.2.1 | Classification of active galactic nuclei (AGN) | 14 |
| 1.2.2 | Disc dynamics and the expulsion of jets | 15 |
| 1.2.3 | Jet models and the SSC model | 17 |
| 1.2.4 | Jets of Mkn 421 and Mkn 501 as seen by microwave telescopes . . | 21 |
| 1.2.5 | Fast variability and other properties of AGN flares | 22 |
| 1.3 | The Gamma Ray Horizon | 24 |
| 1.4 | Theory of air showers | 29 |
| 1.4.1 | Electromagnetic cascades | 30 |
| 1.4.2 | Hadronic cascades | 34 |
| 1.4.3 | Cherenkov light production | 36 |
| .1 | The principle of Cherenkov imaging telescopes | 36 |
| .2 | The HEGRA experiment: An overview | 38 |
| .3 | The HEGRA CT1 telescope | 40 |
| .3.1 | Technical details | 40 |
| .3.2 | The trigger of CT1 | 41 |
| .4 | The All Sky monitor of the RXTE satellite | 41 |
| A | The Analysis of shower images | 43 |
| A.1 | The calibration of the telescope data | 44 |
| A.2 | Monte Carlo Simulation of air showers | 44 |
| A.2.1 | Simulation of the night sky light | 45 |
| A.2.2 | Trigger efficiencies, cut efficiencies and effective areas | 46 |
| A.3 | Gamma/hadron separation methods | 48 |
| A.3.1 | The classical Hillas parameters to describe shower images | 48 |
| A.3.2 | Image cleaning algorithms to remove the night sky background in the camera | 53 |
| A.3.3 | Static cuts and dynamical cuts: Dependence of the Hillas parame- ters on the energy, the zenith angle, the impact parameter and the night sky background | 54 |
| A.3.4 | Background determination by using the ALPHA-plot | 58 |
| A.3.5 | The linear discriminant analysis as a dynamical cut and as a tool to quantify the discrimination power of image parameters | 60 |
| A.3.6 | Comparison of the discrimination power of the LDA and the dy- namical cuts, tested with real Mkn 421 data | 64 |
| A.3.7 | Conclusion about the efficiency of the LDA separation method and an outlook | 69 |

| | | |
|------------|--|------------|
| A.4 | New image parameters and cleaning algorithms | 71 |
| A.4.1 | Introduction of weights in the calculation of Hillas parameters | 71 |
| A.4.2 | The head-tail asymmetry defined in a such way that it overcomes the finite resolution of the CT1 camera | 80 |
| A.4.3 | The problem of truncated images due to the limited size of the CT1 camera and the leakage parameter | 81 |
| A.4.4 | Mountains and islands in the shower image: Difference between electromagnetic showers and hadronic showers | 83 |
| A.4.5 | Improvement in gamma/hadron separation | 88 |
| A.4.6 | Conclusion about the introduction of new image parameters and new image cleaning algorithms | 91 |
| A.5 | Energy estimation by the least squares method | 94 |
| A.5.1 | Conclusion about the energy estimation using the linear least squares method | 95 |
| A.6 | Mispointing of the telescope and its correction | 95 |
| A.7 | Differential flux spectrum calculation | 101 |
| A.7.1 | Determination of the energy excess event distribution | 101 |
| A.7.2 | Unfolding the spectrum | 102 |
| A.7.3 | The spectrum, fitting and reverse check of the result | 105 |
| A.7.4 | Discussion of systematic errors and the reliability of the obtained spectrum | 107 |
| A.8 | Calculation of lightcurve and hardness ratio | 108 |
| A.8.1 | The mathematical background of integrated flux measurements | 108 |
| A.8.2 | Discussion about systematic errors and the reliability of the measured lightcurve | 111 |
| B | Analysis of the flares of Mkn 421 in 2001 | 113 |
| B.1 | Light curve and timing of the flares of Mkn 421 | 113 |
| B.1.1 | The light curve of Mkn 421 as measured by CT1 | 113 |
| B.1.2 | Comparison of the lightcurve to the one measured by the CT-system . | 122 |
| B.1.3 | The 2 keV-12 keV lightcurve measured by the All Sky Monitor of the RXTE satellite | 122 |
| B.1.4 | The discrete correlation function applied to TeV and X-Ray light curves | 124 |
| B.1.5 | Conclusion about the γ -ray/x-ray correlation studies | 133 |
| B.1.6 | The hardness ratio as measured by CT1 in 2001 | 134 |
| B.2 | Spectrum of Mkn 421 | 138 |
| B.2.1 | The spectrum averaged over all flares | 138 |
| B.2.2 | The Crab nebula spectrum for consistency cross check | 141 |
| B.2.3 | Analysis of the Mkn 421 spectrum during different flare states | 141 |
| B.2.4 | Conclusions and a discussion of the results | 147 |
| C | Comparison with Mkn 501 and Conclusion | 149 |
| C.1 | Spectral properties of γ -flares | 149 |
| C.1.1 | Time scales, correlations and jet models | 153 |
| C.2 | Outlook | 157 |
| D | Summary | 159 |
| E | Appendix A: Theory and calculations | 163 |
| E.1 | Verification of the NSB distribution function | 163 |
| E.2 | The synchrotron self Compton (SSC) model | 165 |
| E.3 | Error calculation of the correlation function | 167 |
| E.4 | Re-binning and averaging of flux bins | 168 |

| | |
|---|------------|
| F Appendix B: Lightcurves and ALPHA plots | 169 |
| F.1 The complete daily lightcurve | 170 |
| F.2 The estimation of the background for the spectrum | 182 |

Abbreviations and shortcuts

| | |
|-------|--|
| ACT | Air Cherenkov telescope |
| ADC | Analog to digital converter |
| AGN | Active galactic nucleus |
| ASM | All sky monitor of the RXTE satellite |
| CIB | Cosmic infrared background |
| CMB | Cosmic microwave background |
| DFT | Discrete Fourier transform |
| EAS | Extended air shower |
| EGRET | Energetic Gamma-ray Experiment Telescope |
| FOV | Field of view |
| FSRQ | Flat spectrum radio quasar |
| FWHM | Full width half maximum |
| GRB | Gamma ray burst |
| HEGRA | High energy gamma ray astronomy |
| HV | High voltage |
| NSB | Night sky background |
| LDA | Linear discriminant analysis |
| MC | Monte Carlo simulation |
| NKG | Nishimura Kamata Greisen |
| PhE | Photoelectron |
| QE | Quantum efficiency |
| SNR | Super nova remnant |

Chapter 1

Introduction to the theory and detectors

In recent years Astroparticle Physics has been a field of steady growth and increasing interest. Only since the last 15 years, has one been able to measure and observe phenomena which are completely new and which have significant impact to our picture of the universe, distant galaxies and black holes. In my thesis I will report on the analysis of the large, persistent very high energy gamma-ray (shortcut γ -ray) flaring of the active galactic nucleus **Mkn 421**.

In this chapter I wish to describe the essential theory which is needed for this Thesis. First the properties and the origin of cosmic rays will be summarized. This is followed by a classification and description of the active galactic nuclei (AGNs). A very simple jet model which accelerates the parent particles of very high energy (VHE) γ 's¹ will be described. This is needed to understand the properties of Mkn 421. The very high energy gamma ray absorption by the cosmic infrared background, which might affect the observed spectrum, is quantified and simulated. Then I will explain the various possibilities for detecting cosmic rays and describe the HEGRA experiment. Later in this chapter, Cherenkov telescopes will be discussed, including how they function. Emphasis is put on the HEGRA CT1 telescope which was used to record the data used in this thesis.

1.1 Cosmic rays

Every second about 1000 high energy cosmic particles (integrates flux above 10 GeV) per square meter hit the Earth's atmosphere. Up to an energy of approximately 1 PeV the chemical composition has been measured directly (for an overview see [LON97/1]). Most of them are ionized nuclei. Approximately 90% of them are protons, 9% are alpha particles, a small fraction are ionized nuclei of heavier elements and a fraction of a percent (0.1%) are high energy gammas [Gai90]. Neutrinos (ν 's) are also present but their number is unknown because of their extremely small interaction cross section.

Charged particles are deflected in the intergalactic and galactic magnetic field. Therefore, they no longer point back to their origin. Only neutral particles can be extrapolated back to their sources. Among the neutral particles, neutrons², ν 's and γ 's, only the latter type are sufficiently abundant. γ 's are **messenger particles** which give us information about the source, its flux, spectrum, timing information and about the γ propagation in the path between the source and the observer.

¹Throughout this document the abbreviation ' γ ' refers to a high energy (> 1 GeV) photon.

²Neutrons decay with a life time of 940 s. Still, extremely high energy neutrons ($> 10^{18}$ eV) could reach us before they decay from close objects as the center of our galaxy.

The main questions today are: (1) Where do they **come** from ? (2) What is the **composition** of cosmic rays ? and (3) What are the **acceleration mechanisms** that are able to accelerate particles to these high energies ?

1.1.1 The spectrum of cosmic rays

As of today, it is **not fully known** where the cosmic rays (CR) come from and how they are accelerated to such high energies (in the GeV to PeV energy range). It is commonly agreed that there exist three populations of cosmic rays: (1) Particles emitted by the sun which relatively low energies up to about 10 GeV, (2) galactic cosmic rays which dominate the spectrum up to 1 PeV and (3) extragalactic cosmic rays which have highest energies [LON97/2]. For simplicity I will restrict myself to the latter two types above energies of 10 GeV which are relevant for Cherenkov telescopes. Lets have a closer look at the spectrum of cosmic rays.

Fig. 1.1 shows the all particle spectrum of cosmic rays. The typical spectrum follows a power law and it is usually characterized by a constant called spectral index α :

$$\frac{dN}{dE} \propto E^{-\alpha} \quad (1.1)$$

Of interest is the region around 5 PeV, the so-called knee position, where the spectral index changes from $\alpha \approx 2.7$ to $\alpha \approx 3.0$. The part **below** the knee is believed to be quite well understood [LON97/1]. The dominant portion of the particles is of **galactic origin**. The current belief is that shock wave acceleration in supernovae remnants (SNR) is the major source of galactic CR. Particles and ionized nuclei are emanated by red and blue giants and are boosted to higher energies in the shock fronts of SNRs. The chemical composition of the CR up to the knee can be explained by a combination of intrinsic source composition and a **spallation process** whereby heavier elements are broken down to lighter elements. It is believed that the CR are deflected and **confined** in the magnetic field of our galaxy. By measuring the abundance of radioactive isotopes it has been found that CR are confined from 10^6 to 10^7 years inside our galaxy. This explains the high isotropy of the CR in this energy range.

Above 1 PeV, shock wave acceleration becomes ineffective and the CR **leak out** of our galaxy (leaky box model [LON97/1]) because the galactic magnetic field is not strong enough to confine the particles in our galaxy. The chemical composition has not been measured above the knee and it is not clear as of today where these cosmic rays come from. The **spectral index** of the cosmic rays **above the knee** can be explained by the assumption that very high energy cosmic rays escape from the galaxy. The strongest argument for this theory is the **increasing anisotropy** with increasing energy of the particles [LON97/1]. A large part of the CR up to 10^3 PeV would therefore still be of galactic origin.

Above 10^4 PeV it is widely agreed that these CR must be **extragalactic** since their Larmor radii in the galactic magnet field is larger than the size of our galaxy [Gai90] and can **no longer be confined**. Another argument is that the **anisotropy changes** and that the highest energy particles appear to originate mainly **from high galactic latitudes**, most likely from the **local super-cluster** [LON97/1], while for lower energies the anisotropy points to the **galactic plane**. For the highest energy particles (up to 10^{21} eV) no satisfactory acceleration model exists.

1.1.2 Sources of cosmic rays

Candidates for cosmic accelerators are objects that have significant magnetic fields and/or very large extensions and at the same time have extremely fast moving shock fronts. The most important candidates for the production of high energy CR are the following.

- **Supernova remnants** which accelerate particles in their shock front.

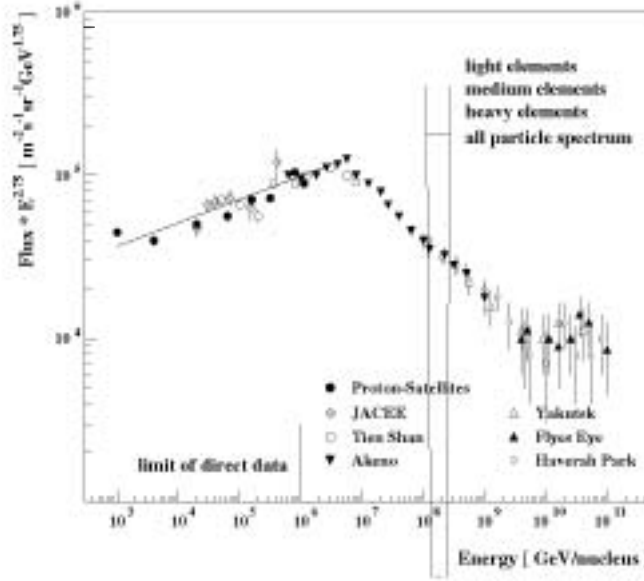


Figure 1.1: All particle differential spectrum multiplied with $E^{2.75}$ for better illustration of the knee at approximately 5 PeV (Taken from [Wie94]).

- **Pulsars** and neutron stars.
- **Active galactic nuclei (AGN)**: Probably super massive black holes with more than 10^6 solar masses that emit plasma jets with high Lorentz factors (up to ~ 10). Shock fronts inside these jets are able to accelerate particles to very high energies.
- **Gamma ray bursts**: Huge explosions of still unknown origin, visible almost uniquely in the soft γ -regime.
- **Binary** star systems **with a neutron star** or a **black hole**.

In this work I will discuss active galactic nuclei (AGN), with focus on Mkn 421 which belongs to the group of BL LAC objects, for which the jet is pointing towards the earth.

1.1.3 γ -rays and γ -ray production processes

As already mentioned, the only particles which are sufficiently abundant and which can be traced back to their origin are γ -rays. Therefore γ -spectroscopy is the method to learn more about the physics of cosmic sources. There are several physical processes which are believed to generate gamma ray photons. These are:

- **π^0 -decay**: High energy protons interact with matter and produce a variety of hadronic particles. Approximately 30% of them are π^0 , which decay almost instantaneously into two gammas (with branching ratio $> 99\%$).
- **Bremsstrahlung**: If a charged particle is accelerated or decelerated (in an electric field), it emits photons. This could be a high energy electron or proton in the Coulomb field of a nucleus or ion. The Bremsstrahlung spectrum of high energy electrons has the same spectral index as the electron spectrum itself, provided that the latter follows a power law.

- **Synchrotron radiation:** This is similar to the acceleration in an electric field: If a charged particle is accelerated (deflected) in a magnetic field, it emits photons. The peak emission of synchrotron radiation is given by:

$$E_{Peak} = 5 \cdot 10^{-9} \cdot H \cdot \gamma^2 \quad (1.2)$$

H is the perpendicular magnetic field component in Gauss, γ is the γ -factor of the electron and the energy E_{Peak} is given in eV. For example, in the relativistic jet of an AGN, the magnetic field is about $H=0.1$ G. The electrons are accelerated by shock-waves up to $\gamma = 10^6$. The peak emission of synchrotron radiation occurs at approximately $E_{Peak} = 500$ eV. One can see that in order to get high energy photons (> 1 GeV), relativistic electrons and a reasonably strong magnetic field are required. This is normally not the case. On the other hand, these low energy photons may produce a dense photon field with high energy electrons that they become a target for interaction: Namely, for **inverse Compton scattering**. This process becomes very important for the generation of ultra high energy gamma rays.

- **Inverse Compton scattering:** Relativistic electrons up-scatter low energy photons to higher energies. The synchrotron radiation and the inverse Compton scattering will be discussed in detail in the section **concerning** the synchrotron-self-Compton (SSC model).

All these processes can take place in active galactic nuclei, which will be described in the following section.

1.2 Active galactic nuclei and the class of BL LACs

In this section I will briefly summarize some relevant features of **active galactic nuclei (AGN)**. The term AGN refers to a class of galaxies which have a **very large mass** in the order of 10^6 to 10^{10} solar masses concentrated in a region of the **size of our solar system**. It is believed that these central objects must be super massive black holes. The energy source of these objects is thought to be converted gravitational potential. There are several different classes and types of AGN which are all believed to be connected by a **single model**, namely the unified AGN scheme [Pad1/99, Pad2/99].

1.2.1 Classification of active galactic nuclei (AGN)

The classification [Pad1/99, Pad2/99, Gui98] is based on the galaxy shape and various physical properties like emission lines, microwave emission spectra and gamma ray emission (See fig. 1.2)

All of these objects are divided in two large groups: Spiral galaxies and elliptical galaxies. Members of the first group are called Seyfert galaxies and these are subdivided into Seyfert galaxies I and II. Type I galaxies have broad emission lines while the latter type galaxies have narrow emission lines. The elliptical galaxies are subdivided, according to their radio emission, in weak and strong radio emitters. Members of the class with weak radio emission are called Radio Quiet Quasars. Members of the class with strong radio emission are again subdivided in two big groups, one with strong and one with weak optical emission lines. The ones with strong optical emission lines are called Radio Quasars, which themselves are subdivided in two groups: **Flat Spectrum Radio Quasars (FSRQ)** and Steep Spectrum Radio Quasars (SSRQ). The first type, having weak or no optical emission lines are grouped into Radio Galaxies having no gamma emission, while the **BL LAC** objects which have some gamma emission, into a group with flat radio spectrum and optical polarization. Finally, BL LACs and FSRQ together form the class of **Blazars**. All blazars emit γ -rays.

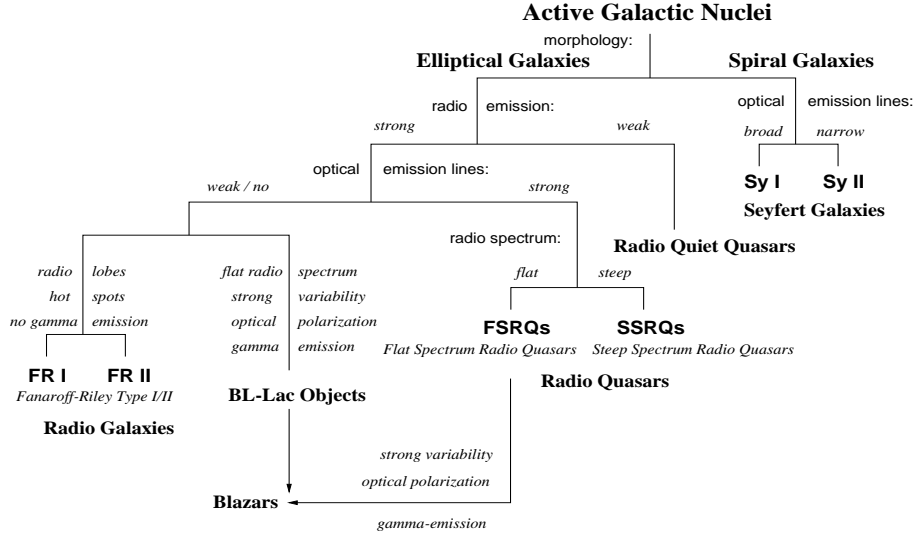


Figure 1.2: Classification of AGN, taken from [Böt97]

It has been tried to relate all these different classes and subdivisions to a general picture of AGNs. Fig. 1.3 shows a schematic sketch. At the center of each AGN is a **super-massive black** hole between 10^6 to 10^{10} solar masses surrounded by a **highly relativistic rotating accretion disc** [Liv02]. Due to **friction** the disc heats up to temperatures in the order of keV, thus transforming the gravitational potential into thermal energy. The plasma emits a **thermal spectrum** which peaks in the (soft) **x-ray** region. Photons emerging from the disc **excite** atoms and molecules in gas clouds, either close to the disc, which yields strong Doppler broadened optical emission lines, or further away from the torus, which produce narrow lines (because they are colder and have smaller velocities).

The different spectral differences are believed to originate from **different observation angles** and also from **different physical parameters**, like the **accretion rate** and the **spin** of the black hole.

Sometimes there are strongly collimated, **highly relativistic jets** or blobs emitted perpendicular to the accretion disc from the poles of the black hole. The **radio emission is related to synchrotron emission** of relativistic (i.e. electrons) particles in the jet. The γ -emission is also believed to be produced by the jet. Since the jet has relativistic velocities, the radiation is beamed in forward direction and the γ -emission can only be seen if the observation angle to the jet is less than $\theta \sim \frac{1}{\Gamma}$ (-> Blazars), where Γ is the Lorentz factor of the jet or blob.

The acceleration mechanism is **yet not fully understood**. The general ideas are presented in the next section.

1.2.2 Disc dynamics and the expulsion of jets

The accretion disc plays an **important role** in the emission of jets. The **key point** seems to be the **collapse** of the disk. The theory of accretion discs predicts that the **disc becomes unstable** when it overheats and becomes optically too thick (Eddington limit) such that the thermal energy can no longer escape in the form of electromagnetic radiation [Mag01]. At this points the disk collapses and the inner part of the accretion disc falls into the black hole [Mei01].

Recently, hints have appeared of a **connection** between the **collapse** of the accretion disc and the **ejection** of a jet [Mar02]. This phenomenon has been observed in the case of 3C120, a radio quasar. The collapse of the accretion disc has been associated with the

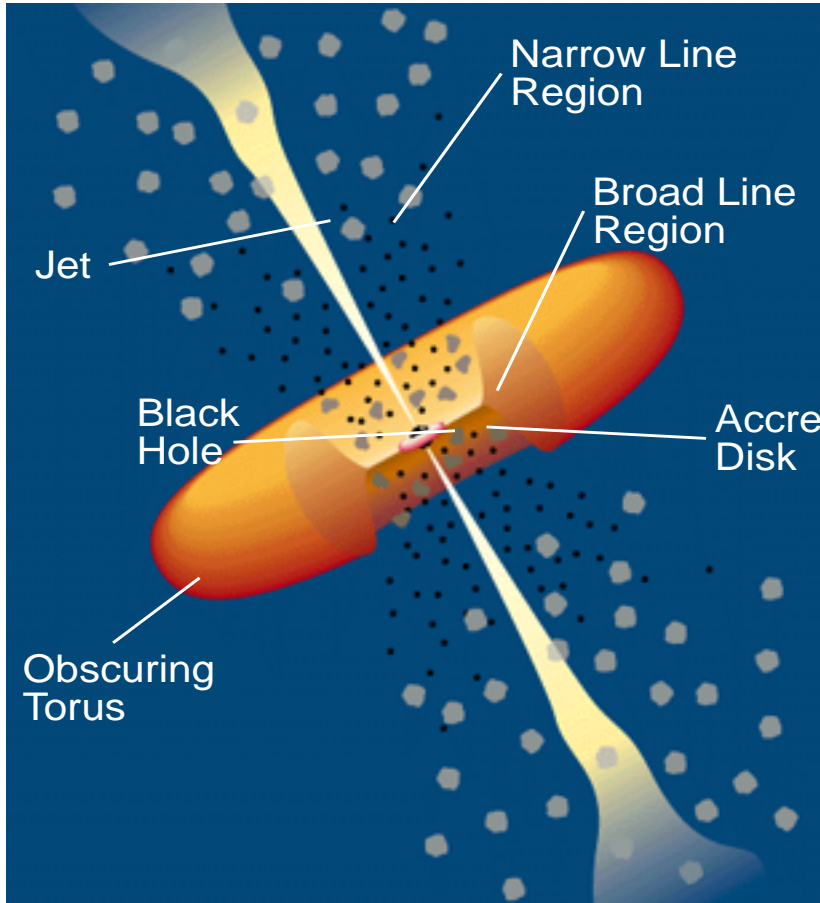


Figure 1.3: The AGN model is supposed to unify the different classes and subdivisions of AGN into one general picture. At the center of each AGN is a **super-massive black hole** between 10^6 to 10^{10} solar masses surrounded by a **highly relativistic rotating accretion disc** [Liv02]. Due to **friction** the disc heats up to temperatures in the order of keV, thus transforming the gravitational potential into thermal energy. The plasma emits a **thermal spectrum** which peaks in the (soft) **x-ray** region. Photons emerging from the disc and **excite** atoms and molecules in gas clouds, either close to the disc, which yields strong Doppler broadened optical emission lines, or further away from the torus, which produce narrow lines (because they are colder and have smaller velocities). The different spectral differences are believed to originate from **different observation angles** and also from different physical parameters, like the **accretion rate** and the **spin** of the black hole. Sometimes there are strongly collimated, highly relativistic jets or blobs emitted perpendicular to the accretion disc from the poles of the black hole. The **radio emission is related to synchrotron emission** of relativistic (i.e. electrons) particles in the jet (Picture taken from [Pad95]).

so-called **x-ray dip**, which is a spontaneous and significant decrease in the thermal (soft) x-ray emission of the disk. The soft x-rays have been clearly identified by an iron emission line, believed to originate from the inner part of the accretion disc. The dip is only seen in the soft x-ray emission. A **clear correlation** between the **x-ray dip** and the **ejection** of a radio blob has been observed.

To get a better understanding of the acceleration mechanism of jets, a **laboratory experiment** was setup [Hsu02]. The system of a central object and an accretion disk was simulated by a plasma (in form of a disc) together with a magnetic field generated by a magnet and an electric field between the central object (a round electrode) and the disc (an electrode ring). The jet was ejected when the electric field was switched on. In this experiment the jet was **magnetically driven** and also magnetically **collimated**. The experiment also showed that jets with helicity appear naturally in such a system (See Fig. 1.4).

Furthermore, **general relativistic magnetohydrodynamic (MHD) 3-D simulations** of the accretion-disk/black-hole system have shown that jets are a natural consequence of a rotating disk in the **presence** of a magnetic field [Mei01, Kud99, Koi02]. The simulations seem to suggest that mainly **very fast rotating** Kerr black holes (mass M) with spins from $a = 0.90 M$ up to $a = 0.95 M$ (maximally rotating is $a = 1.0 M$) are able to accelerate jets up to Lorentz factors of $\delta = 10$. The accelerated plasma most likely originates from the **outer halo** of the accretion disk. The jet is **magnetically driven** and also magnetically **collimated**. The particles accelerating from the plasma are **most likely electrons**. Heavier particles and ions are slower and remain in the disk halo [Mag01]. This would imply that the jet mainly consists of **electrons** and **electromagnetic radiation**.

Evidence for the **collimation** of the jet at a distance to the nucleus between 30 and 100 Schwarzschild radii was recently observed in the radio galaxy M87 by J. Biretta et al. [Bir02]. During jet collimation, very close to the black hole, the jet opening angle appears to increase while at larger distances it decreases.

Other theories claim that the black hole acts like a **huge dynamo** in a magnet field generated by the accretion disc. The event horizon behaves like an electric conductor and builds up an electric field between the equator of the black hole and its pole. The static magnetic and electric field densities (**Poynting flux**) reach such a strength that e^+e^- pairs are created **out of the vacuum**. These electrons are accelerated by the electric field and focused by the magnetic field [Mag01]. Such jets are purely electromagnetic.

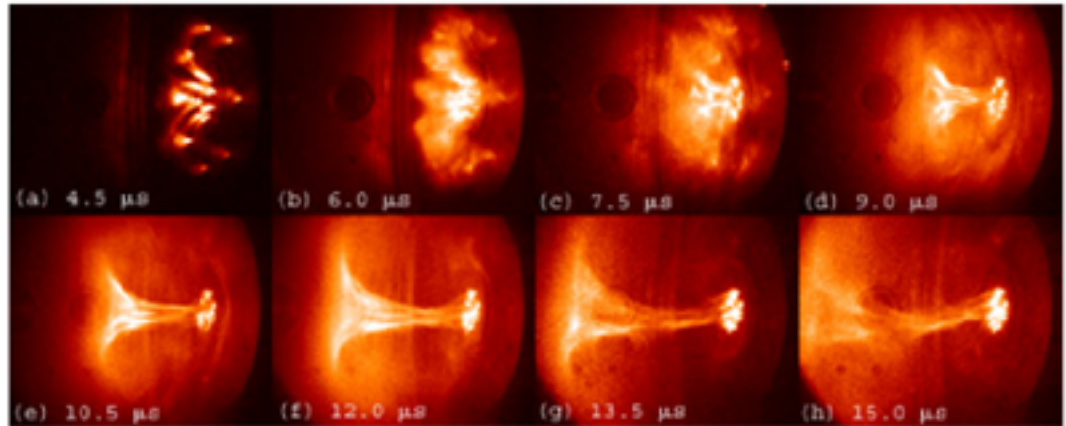
Future measurements and simulations will clarify the question whether the jet only consists of electrons or if hadrons are present as well.

1.2.3 Jet models and the SSC model

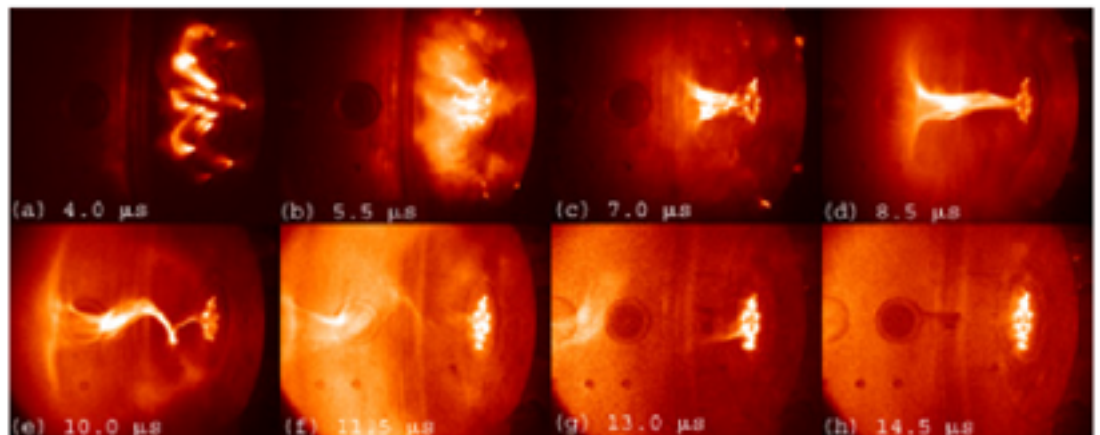
It has been tried to explain the γ -emission by two different models:

1. The **synchrotron self Compton (SSC) model** attempts to explain the production of very high energy gammas (TeV range). An elegant and apparently natural way to explain the existence of very high energy gammas is by inverse Compton up-scattering of soft photons that are produced by the same high energy electrons that are involved in the scattering by synchrotron radiation.
2. In **hadronic jet models** the jet contains hadrons (e.g. protons) which produce π^0 's in collisions. These π^0 's decay into two γ s and the high energy γ emission can be explained in this way. This model also would explain the **existence** of hadronic high energy cosmic rays.

Even that it seems very **probable** that a jet also contains a hadronic component, in the moment it seems that the (at least the pure) hadronic model has been **discarded** because the shape of the observed γ -spectrum to its theoretical prediction. On the contrary, the SSC model fits the shape of the observed spectrum very well. In this work I will restrict myself to the SSC model only.



(a) Development of a jet without helicity



(b) Development of a jet with helicity

Figure 1.4: Images of a laboratory experiment to designed to simulate jet emission which show the expulsion and development of a jet in a series of pictures. Plot a) shows a straight jet and plot b) shows a jet which develops a helical instability. Taken from [Hsu02].

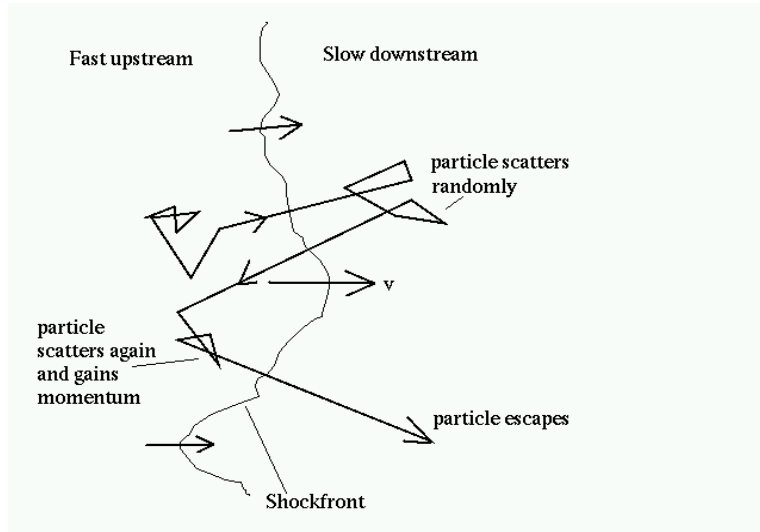


Figure 1.5: Illustration of the shock acceleration mechanism. The particle is scattered several times, forth and back over the shockfront. In each cycle it gains energy due to the movement of the shockfront.

The mechanism necessary to efficiently accelerate charged particles (e.g. electrons) to extremely high energies ($> 1 \text{ TeV}$) is believed to be the so-called shock wave acceleration [Gal02].

Shock wave acceleration model

The just mentioned **shock waves** or shock fronts are naturally present in jets and supernovae remnants (SNR). Particles are randomly **scattered by local magnetic irregularities** (Alfvén- and hydromagnetic waves [LON97/2]), thus passing many times from downstream of the shock front into the upstream interstellar medium (or if the shock front is inside the jet, from the downstream shock over to the slower upstream plasma in the jet) and back (see fig. 1.5). At **every cycle** the particle will **gain energy** due to the fast movement of the downstream shock [Gal02]. For nonrelativistic shocks the following formula shows the energy gain compared to the initial energy, averaged over all inclination angles.

$$\left\langle \frac{E_f}{E_i} \right\rangle = 1 + \frac{4}{3} \beta_{rel} \quad (1.3)$$

β_{rel} is the velocity of the jet in units of c . The particle has a **probability to escape** the acceleration front volume by being scattered away from the shock front. Taking this probability into the calculation the resulting spectrum has a **power law** shape. In nonrelativistic shocks the angular distribution of the movements is uniform and for a strong nonrelativistic shock this leads to power law spectra with spectral index $\alpha = 2$.

$$\frac{dN}{dE} \propto E^{-\alpha} \quad (1.4)$$

For ultra relativistic shocks, which is the case for jets emitted by AGNs, the escape probability and the average energy gain per cycle is more complicated due to the relativistic movement. The angular distribution of the high energy charged particles is not isotropic anymore. In [Gal02] it has been demonstrated, that by assuming different scenarios, the spectral index for ultra relativistic shocks is in the range of $\alpha=2.2$ to $\alpha=2.3$.

A very important question concerns the **maximum energy** that can be reached by this mechanism. The hard limit of the maximum energy depends mainly on two aspects.

1. The radius of the emission region must be **larger** than the Larmor radius of the particle.

$$E_{max} \simeq qB\gamma R_{jet} \quad (1.5)$$

B is the magnetic field in the jet, R_{jet} is the radius or jet scale, q is the charge of the accelerated particle and γ is the relativistic gamma factor of the particle. According to Equ. 1.5 for a jet radius of $R_{jet} = 0.01$ pc = $3 \cdot 10^{14}$ m, a gamma factor of $\gamma = 10$ and a magnetic field of $B = 0.1$ G the absolute maximum energy is in the range of 10^{14} eV or 100 TeV. These numbers give the order of magnitude that is generally expected in such jets.

2. The electrons are constantly being **cooled down** due to two effects and limit the maximum reachable energy if the cooling becomes faster than the acceleration:
 - (a) Emission of **synchrotron radiation** (which depends on the magnetic energy density u_B in the jet)
 - (b) **Inverse Compton** scattering (which depends on the soft photon density u_{soft}).

The SSC model and relativity

As already mentioned, the idea behind the Synchrotron Self Compton model is that the observed high energy γ 's are produced by an **inverse Compton up-scattering** of low energy photons (UV and soft x-rays) by high energy electrons. The required dense **soft photon field** is assumed to be produced via **synchrotron emission** by the same high energy electrons by magnetic irregularities in the jet (the relevant parameter is the magnetic energy density u_B). The SSC model is described in detail in Appendix A.

As an alternative (which is not SSC), the soft photons could also originate from the **accretion disc** if the latter is not too far away from the blob. This possibility will be discussed in the last chapter.

The **typical SSC** model spectrum consists of two emission peaks (see Fig. 1.6). One **synchrotron peak** (the soft photon field) which peaks in the UV or soft x-rays region and one **inverse Compton peak** which peaks in the GeV-region.

Due to the **relativistic** motion of the source (along the jet axis), the emission intensity is **boosted** in the direction of motion and becomes stronger and more energetic for an observer for whom the jet approaching as compared to an observer in the moving (blob) frame [Mag01]. The so-called beaming effect is characterized by the Doppler factor δ :

$$\delta = [\gamma (1 - \beta \cos \vartheta)]^{-1} \quad (1.6)$$

where β is the velocity in units of c with

$$\beta = \sqrt{1 - \frac{1}{\gamma^2}} \quad (1.7)$$

where γ is the relativistic Lorentz factor of the motion and the observer sees the jet at an angle ϑ .

The **Lorentz-transformations** of the local comoving jet system (whose observables are primed here, eg. dt' , $I'(\nu')$) relative to the distant observer system (whose observables are unprimed, eg. dt , $I(\nu)$) yield:

- All longitudinal **length scales** and **time scales** must be divided by the Doppler factor δ :

$$dt = \delta^{-1} dt' \quad (1.8)$$

$$dx = \delta^{-1} dx' \quad (1.9)$$

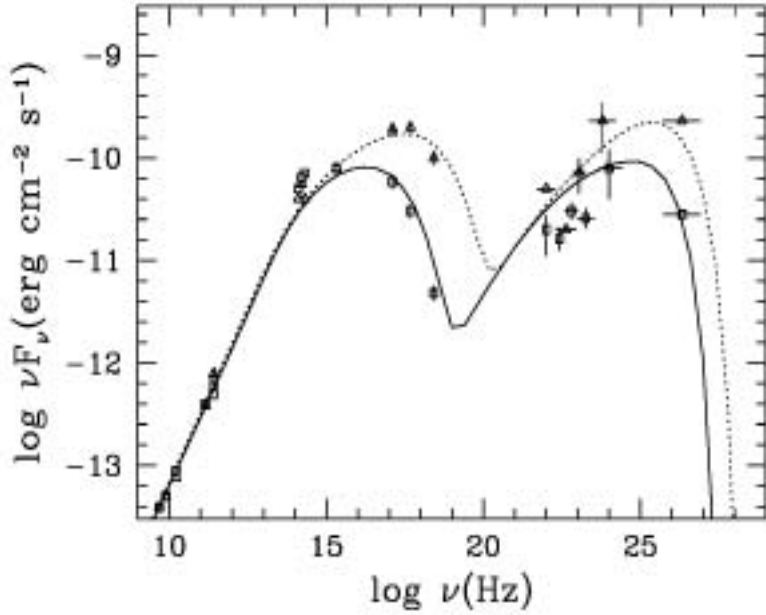


Figure 1.6: This figure shows an example of the double peak structure of a possible SSC model. Here the low and high states of the multi-wavelength spectrum of Mkn 421 have been fitted with a SSC model using a laminar geometry for the emission region. Taken from [Mas99]. Parameters used: variability time scale $t=500$ s, with a Doppler factor of $\delta = 20$ (for low state, while for high states δ is by a factor four higher), with a magnetic field of $B=0.4$ G, and a maximum electron energy of $\gamma_{max} = 1.4 \cdot 10^5$.

- The **intensity** scales with δ^3 as:

$$I(\nu) = \delta^3 I'(\nu') \quad (1.10)$$

where $\nu = \delta \cdot \nu'$ and ν is the photon frequency. The opening angle of the light cone due to relativistic beaming is

$$\theta \simeq \tan \theta = \frac{1}{\gamma} \quad (1.11)$$

where theta is the opening angle of the cone and γ the Lorentz factor of the blob. Any (γ -) radiation emitted by the jet is beamed in forward direction.

1.2.4 Jets of Mkn 421 and Mkn 501 as seen by microwave telescopes

The jet properties are discussed on the basis of the two AGNs **Mkn 421** and **Mkn 501**. The former is subject of this thesis and the latter will be used later for comparison.

The contemporary picture of a jet is a blob of relativistic particles that is ejected by the AGN. The **Lorentz factor** has been estimated for the case of many Blazars and radio galaxies by measuring the **superluminal motion** of the blob seen by radio telescopes. Radio telescopes have the necessary angular resolution to a precision of miliarcseconds, a resolution that is impossible to achieve for optical wavelengths. The general conclusion is that the Doppler factor of most blazars and radio galaxies is typically $\delta = 10$ [Pad2/99].

Superluminal motion is a **natural effect** of relativity in which the blob moves at angles of approximately 30° - 60° in direction to the observer, who measures an apparent speed that is faster than light [Mag01]. The observed speed of the motion is:

$$\beta_{ob} = \left| \frac{\vec{n} \times (\vec{\beta} \times \vec{n})}{1 - \vec{\beta} \cdot \vec{n}} \right| \quad (1.12)$$

$$= \frac{\beta \sin \phi}{1 - \beta \cos \phi} \quad (1.13)$$

where \vec{n} is the observer direction, ϕ is the observation angle, $\vec{\beta}$ the velocity of the blob in the observer frame and β_{ob} is the apparent velocity observed by a telescope.

It is believed that the jet has a very high Lorentz factor **immediately after** its expulsion and collimation. Later it rapidly **cools down** by emission of synchrotron and inverse Compton radiation. The Lorentz factor of the blob decreases with increasing distance from the nucleus. At high Lorentz factors it radiates predominantly in the form of hard x-rays and (i.e. BLAZARS) in γ -rays. Eventually, when the jet is much further away from the nucleus and it has cooled down significantly, the jet emits synchrotron radiation in the microwave energy range at which time it transparent to microwaves. **Only then** will it become **visible in the radio** frequency range [Mar02]. At the point when the jet becomes visible to radio telescopes its distance from the AGN is already hundreds of parsecs.

Both objects, Mkn 421 and Mkn 501, have been observed with **radio telescopes** (see Fig. 1.7). As previously explained, it is assumed that the jets of these two objects move in the direction of the observer within an angle of $\theta \sim \frac{1}{\gamma} \sim 0.1 \text{ rad} \sim 6^\circ$ ($\gamma = 10$) from the fact that we see γ -radiation that is emitted in the forward direction. Unfortunately, the exact observation angle is **unknown**. However, we do know that the movement is not exactly in the line of sight because moving blobs with superluminal velocity have been observed. These blobs are relatively slow. Mkn 421 blobs exhibit a velocity of only $v = 2 \pm 0.1 c$ and Mkn 501 blobs have velocities of approximately $v = 2.5 \pm 0.1 c$ [Mar99]. These **slow superluminal velocities** of the radio blobs have two explanations:

1. The jet initially had a **higher** bulk Lorentz factor of close to ten when it radiated x-rays and γ -rays (by synchrotron and γ -radiation emission) and subsequently **cooled down rapidly**, more rapidly than other typical radio galaxies. Later the observed radio blob only shows a Lorentz factor **of approximately 3**.
2. The **observation angle is very small** such that the superluminal motion has only small values between 2.0 and 2.5. This would allow a high Lorentz factor of the blob **close to 10**.

It should be mentioned that the jet structure of both objects is significantly different. This can be seen for example in the magnetic field (can be seen in the polarization of the radio emission [Mar99]) which is perpendicular to the jet in case of Mkn 501 and for Mkn 421 the magnetic field is parallel to the jet.

1.2.5 Fast variability and other properties of AGN flares

As of today, several Blazars which emit gamma rays in the TeV range have been detected. The most significant of these are Mkn 501, Mkn 421, 1ES1426, 1ES2344 and 1ES1959, while astronomers have discovered about 60 AGN in the GeV range mainly by the EGRET satellite (see Fig. 1.8). All the known GeV Blazars are radio loud. The radio emission is assumed to be synchrotron radiation of very high energy particles (mostly electrons but with a possible (weaker) contribution from protons) in the jet. The synchrotron emission extends up to the soft x-ray where it can be detected with satellites like ASCA or RXTE. Synchrotron radiation hints to the SSC model.

A very important feature of the AGN flares is its extremely fast variability. Mkn 501, assumed to be a black hole of 10^8 solar masses, and Mkn 421, smaller with approximately 10^6 solar masses are rather extended objects with Schwarzschild radii of the order of 1 AU and 1/100 AU respectively and with distances from the black hole to the accretion disc between 10 and 100 Schwarzschild radii. The distances from the black hole to the jet extend even further, with Schwarzschild radii at the order of 10^4 to 10^{10} . **The observed variability is very rapid**. Typical timescales are **a few hours for Mkn 501** and about **15**

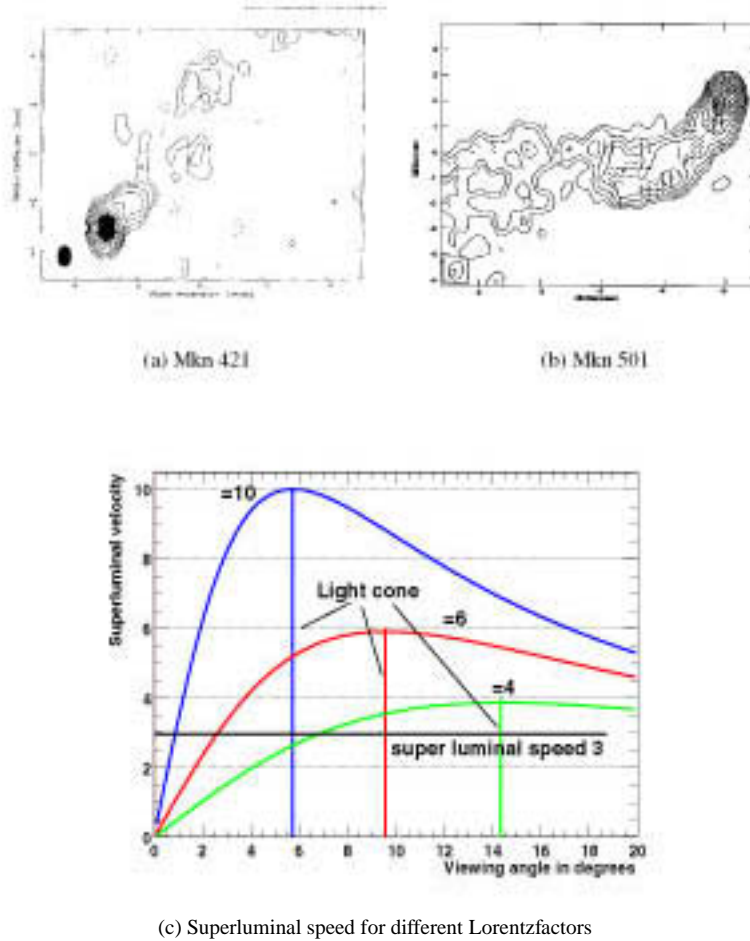


Figure 1.7: Shown here are VLBA radio images of the two objects Mkn 421 and Mkn 501, taken at 15 GHz. Picture a) shows Mkn 421, taken on July 1997 and picture b) displays Mkn 501, taken on August 1997. Mkn 421 is very core-dominated which could be due to a small observation angle. Mkn 501 shows a bending in the jet of almost 90°. Both radio jets show superluminal motion exceptionally slow for typical radio galaxies. Mkn 421 blobs have approximately a velocity of $\beta_{obs} = 2.0c$ and blobs of Mkn 501 have approximately $\beta_{obs} = 2.5c$. These plots were taken from [Mar99]. Plot c) shows the superluminal speed as a function of the observation angle (in degrees) for three different Lorentz factors ($\gamma=4$, $\gamma=6$ and $\gamma=10$). The vertical line shows the position of the light cone. Since from these two objects γ -emission is observed the actual observation angle must be smaller than this limit.